Extensible High Force Manipulator For Complex Exploration

Josie Hughes[1], Cosmio Della Santina[1] and Daniela Rus[1]

***Abstract*— The development of compliant robotic manipulators which can show length change, compliance and dexterity could assist many challenging applications. Potential applications range from dexterous manipulation, robotic surgery or exploration of challenging environments. Despite significant developments in both fabrication and control approaches for continuum body manipulators, there have been few demonstrations of continuum body systems which display all these properties. We present a method for fabricating a continuum manipulation which shows extension, high force movements and a range of dexterous position. This approach uses 3D printing to create a flexible rack and pinion system. These high torque mechanisms are mounted at points along the 3D printed tracks to allow complex shape control of the continuum system. A controller has been also been developed based on a Piecewise Constant Curvature approximation to allow the position of the tip of the manipulator to be controlled, and motion paths to be followed. In this work, we show the force capabilities of this manipulator and demonstrate how multiple segments can be created for more complex movements.**

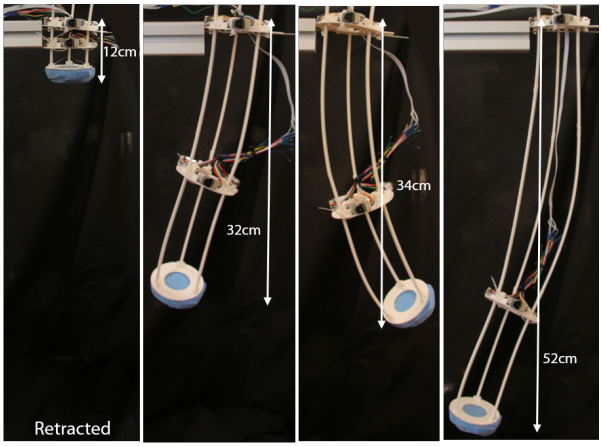

Fig. 1. Images of the manipulator in the retracted position (left) and the expanded position indicating the range of motion and compliant behavior which can be achieved with a two-segment system.

I. INTRODUCTION

Animals show a range of compliant manipulators which enable highly complex and dexterous interactions with the environment through compliant interactions, growth and many other mechanisms. Examples include elephant trunks which shows huge maneuverability and dexterity whilst also having the ability to apply high forces to break or tear foliage [1], or octopus legs which show highly compliant behaviors which enabling many life critical activities [2]. The dexterity, and exploration capabilities of these biological manipulation systems would be extremely beneficial for robotic systems.

Developing such compliant continuum body systems could enable manipulators which can reach into hard to access locations, and locate and retrieve objects. This would demonstrate capabilities that would start to come close to those of animals, for example, mirroring human capabilities to reach into a bag and extract a specific item. These capabilities would enable many challenging applications ranging from exploration of complex environments, manipulation in challenging obstructed environments, robotic exploratory surgery and more [3], [4].

Due to the potential for such technologies to show high impact solutions, there has been an increasing focus on the development of soft manipulators which use continuum body structures [5]. Many different methods for fabrication and control of such structures have been investigated. This includes creating soft structures with pneumatically operated chambers [6], [7], using particle jamming to modulate the stiffness across the continuum body [8], [9], or developing tendon driven segmented continuum arm structures [10]–[12]. Another approach is vine robots, which can achieve incredible length change, however, controlability and motion planning for such robots is challenging [13]. Other biologically inspired approaches include 'growing' robots. A number of growing robots have been developed which show direction controllable growth [14], [15], however growth is often slow and not reversible. Additionally growth from the tip of the structure has been shown [16].

In addition to the physical design and fabrication of continuum body structures, the control and planning poses another challenge [17]. Due to the compliance, the structures can undergo high complex interactions. Approaches to controlling the position of continuum body structures include using model-free self-supervised learning techniques [18], constant curvature models [19] or other models such as the Cosserat approach [20] have been demonstrated.

Despite the significant advances in soft robotics, there are limitations to the maneuverability and extensibility of many existing systems. Thus, we aim to create a continuum structure manipulator which can show extensibility and also curvature in 3D space to allow exploration and manipulation, whilst also showing high force capabilities.

To achieve this, we create a tri-flexible rack and pinion manipulator structure, inspired by previous work using tri-tube structures for a climbing robot [21]. In this we use 3D printed flexible racks, where the directional stiffness is designed to achieve the deformations required for exploratory

[1] All authors are with the Distributed Robotics Lab, CSAIL, MIT. josieh@mit.edu, cosimodellasantina@gmail.com, rus@mit.edu.

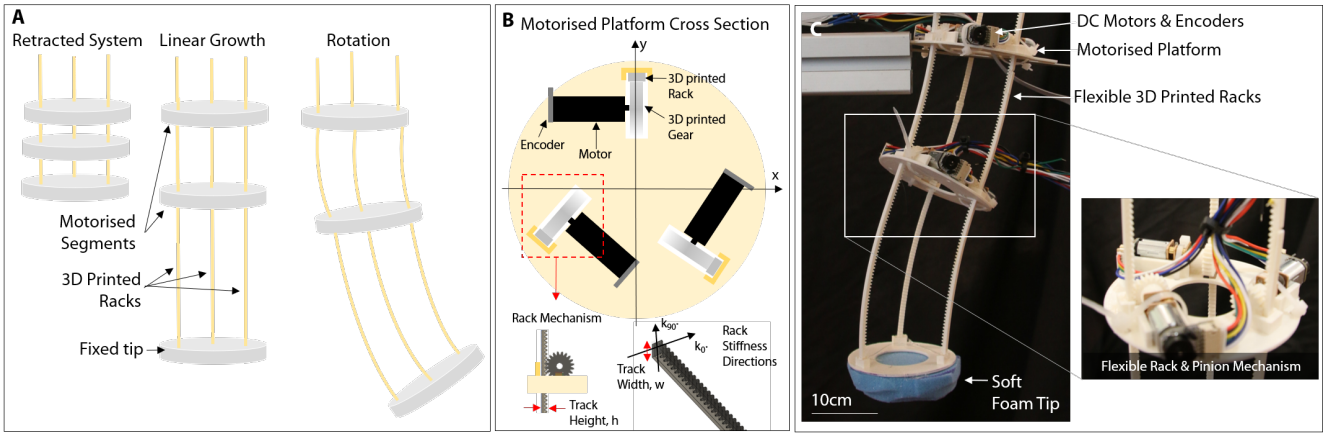

Fig. 2. (A) Diagrammatic representation of the manipulation system, showing how the mechanism can be we used to achieve both growth and change in posture, (B) Diagram showing the motorized platforms, and showing the co-ordinate system for measuring stiffness, and (C) labeled photographs of the manipulator.

movements. In addition, we have developed an open-loop controller to set the motion path of the tip of the manipulator. This allows for highly dexterous movements in 3D space, a substantial length change (with upto 500% length change demonstrated), and high force movements. Fig. 1 shows the retracted system and the extended version in various poses, showing the 3D printed backbone structure of the continuum body manipulator.

In this work, we demonstrate and characterize the capabilities of a single segment of the manipulator, showing the forces which can be applied, the performance of the controller and the range of motion. We also demonstrate how this approach can be used to create multi-segment systems which allow exploration of large areas.

In summary, this paper makes a number of contributions:

- A flexible rack and pinion design for extensible continuum body structures, building on [21], and the design for 3D printable flexible racks, with the various trade-offs in mechanical behavior identified
- Piece-wise Constant Curvature Control methods for this structure to allow the motion of the tip of the structure to be accurately controlled
- Demonstration of the system and testing of both a single segment, and a multi-segment system.

In this paper Section II describes the design and control methods for the manipulation system. Section III presents the experimental setup and fabrication approaches, with Section IV showing the experimental results including characterization and demonstration of a single segment and demonstration of a multi-segment manipulator. Finally, the paper concludes with a discussion reviewing the contributions of this work and scope for future work and applications.

II. METHODS & DESIGN OVERVIEW

A. Actuation System

The actuation system consists of a compliant tri-axial rack and pinion system. Flexible 3D printed rack elements form the tri-axial backbones of the system with segments housing the motor and gear mechanisms, mounted along these flexible racks. In this way, multiple moving platform segments can be attached along the 3D printed racks to enable both considerable extension and change in length, and also change orientation within 3D space. The design and the mechanisms developed are highlighted in Fig. 2.

B. 3D Printed Tracks

The range of movement and also the strength of the system is determined by the material properties of the flexible rack. The racks are 3D printed; by printing in a way such that the layers run along the long axis of the racks (i.e. the teeth are normal to the bed of the printer), the tracks show flexibility and provide some elastic behavior. If the racks were printed in other directions, due to the internal strain incurred on printing they are brittle, and snap without deforming elastically. 3D printing of flexure based systems is an approach which has been investigated as a method of fabricating soft or compliant systems using well understood 3D printing techniques [22], [23].

The racks are parameterised by the height and width (Fig. 2B). By changing these geometrical parameters the anisotropic stiffness can be varied. The anisotropic stiffness behaviors must allow bending in various axes, whilst also having sufficient stiffness to apply force and not buckle or break.

To investigate the anisotropic stiffness that can be achieved, tracks of different properties were printed, and the stiffness along the 0 degree and 90 degree plane (as denoted on Fig. 2B) measured. The stiffness was measured by performing a 3 point bend test using an Instron machine. The force that must be applied to achieve a given bending deformation was measured, and thus a indication of the bending stiffness, the force per unit of bending distance can be found. Thus, the bending stiffness is defined by:

$$k_\theta = F/x \tag{1}$$

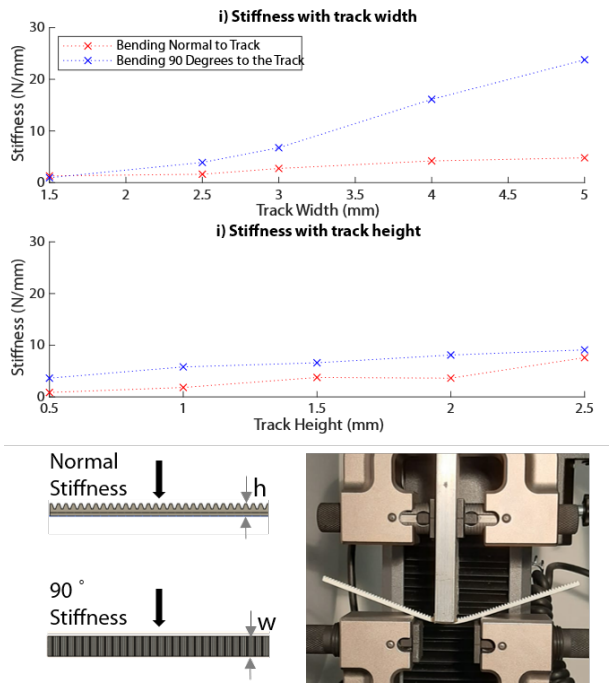

Fig. 3. Variation in the bending stiffness of the track when the geometrical properties (width and height) of the 3D printed rack system is varied.

where x represents measured displacement when a force F was applied. This was measured in the case of F=5N, a condition which could be typical for the system.

The measured bending stiffness for tracks of different geometrical values is shown in Fig. 3 with still images of bending tests also shown. The results show that the track width significantly increases the bending stiffness in the direction 90 degrees to the track whilst showing minimal increase in bending normal to the track. To maximize the force that can be applied whilst ensuring the tracks will deform both along the 0 and 90 degree axis, tracks should be choose where the stiffness is both directions is as close as possible, thus, where $k_{\theta=0} = k_{\theta=90}$. Thus, the track width should be minimized to keep these bending stiffness in the two axes as similar as possible.

In addition to the directional stiffness profile, another key characteristic is the maximum bend radius that can be achieved. The larger the bend radius, the greater the range of motion that can be achieved. Fig. 4 shows the maximum bend radius that can be achieved before break for the 3D printed racks with different width and height parameters. Fig. 4 also shows some images of the rods undergoing bending, highlighting the range of bend radius that can be achieved using 3D printing. In particular (D) shows a highly flexible rack, which is fully flexible. It can be seen that the track width has a significant impact on the maximum radius of curvature, with an increase from 2.5mm to 3mm, decreasing the curvature by almost 50%.

Using these experimental results tracks were chosen to provide a trade-off between maneuverability, range of movement, and applicable force. These tracks were 2.5mm in width, and 2.5mm in height.

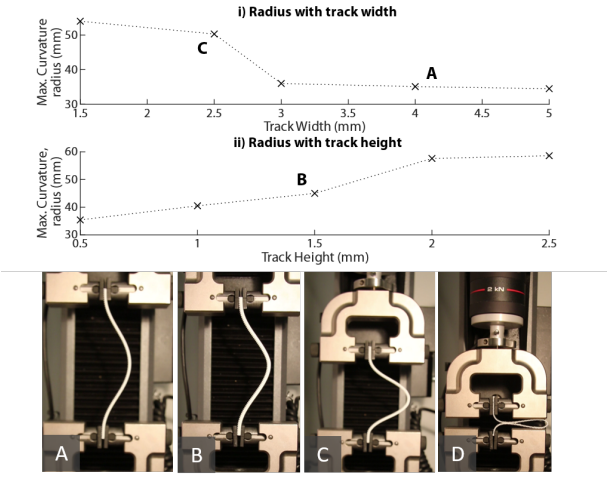

Fig. 4. Variation in the maximum bend radius that can be achieved with racks of different geometrical properties.

C. Kinematic control

Consider a serial interconnection of n of the proposed modules. Its configuration can be expressed univocally under Piecewise Constant Curvature approximation [24], using the Δ-parametrization introduced in [25]. The posture of each segment is therefore described by $\Delta_i = [\Delta_{\mathrm{x},i}, \Delta_{\mathrm{y},i}, \delta L_i]^{\mathrm{T}} \in \mathbb{R}^3$. $\Delta_{\mathrm{x},i} = L^{\Delta}_{2,i} - L^{\Delta}_{1,i} \in \mathbb{R}$ measures the bending in the direction of the local x axis, $\Delta_{\mathrm{y},i} L^{\Delta}_{4,i} - L^{\Delta}_{3,i} \in \mathbb{R}$, the bending in the direction of the local y axis, and $\delta L = \frac{1}{4}\sum_{j=1}^{4} L^{\Delta}_{j,i}$ the overall elongation of the segment - with $L^{\Delta}_{j,i}$ defined as in Fig. 5. $\Delta_i = [\Delta_{\mathrm{x},i}, \Delta_{\mathrm{y},i}, \delta L_i]^{\mathrm{T}}$ can be retrieved from the actuators positions $[L_{1,i}, L_{2,i}, L_{3,i}]^{\mathrm{T}}$, using the following affine map

$$\begin{bmatrix} \Delta_{\mathrm{x},i} \\ \Delta_{\mathrm{y},i} \\ \delta L_i \end{bmatrix} = M_i \begin{bmatrix} L_{1,i} \\ L_{2,i} \\ L_{3,i} \end{bmatrix} - \begin{bmatrix} 0 \\ 0 \\ L_{0,i} \end{bmatrix}, \tag{2}$$

with

$$M_i(\phi_i) = \begin{bmatrix} -\frac{2\cos(\phi_i)}{3} & \frac{2\cos\left(\phi_i+\frac{\pi}{3}\right)}{3} & \frac{2\cos\left(\phi_i-\frac{\pi}{3}\right)}{3} \\ \frac{2\sin(\phi_i)}{3} & -\frac{2\sin\left(\phi_i+\frac{\pi}{3}\right)}{3} & \frac{2\cos\left(\phi_i+\frac{\pi}{6}\right)}{3} \\ \frac{1}{3} & \frac{1}{3} & \frac{1}{3} \end{bmatrix}, \tag{3}$$

where ϕ_i is the angle between the segment connecting L_1 with the center of the segment, and the local x axis (see Fig. 5). We call $\Delta \in \mathbb{R}^{3n}$ the variable collecting all the Δ_i, $M \in \mathbb{R}^{3n\times 3n}$ the block diagonal matrix obtained by collecting $M_1, \ldots, M_n$, and $\Delta_0 \in \mathbb{R}^{3n}$ the vector such that $\Delta(L) = ML - \Delta_0$.

Given a desired position of the robot's tip x_{d}, our goal is to find a suitable solution of the following inversion problem

$$\min_{L\in\mathbb{R}^{3n}} ||x_{\mathrm{d}} - h(\Delta)||, \quad \text{s.t. } L \in [0, L_{\max}]^{3n}, \tag{4}$$

where h is the direct kinematics mapping the robot configuration to the corresponding tip position in Cartesian

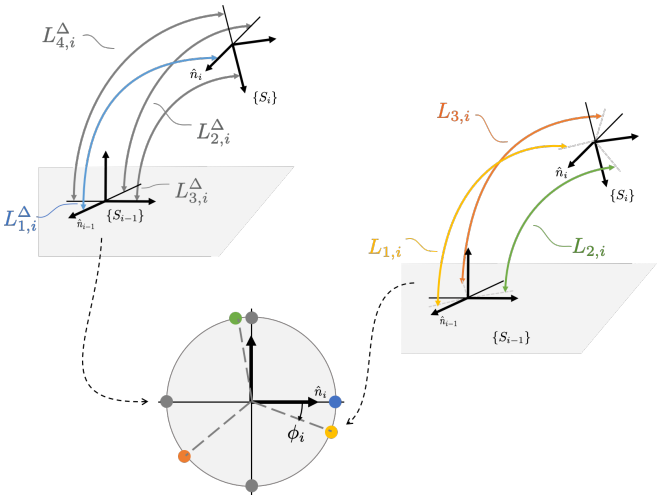

Fig. 5. Kinematic description of the $i-$th segment. The left side of the figure shows the four main arcs used the define the Δ-parametrization. The right side shows the three arcs of which we can decide the length through actuation. The center of the picture reports a cross-section of the segment, to better show the relative position of the seven arcs.

coordinates. We propose to solve this problem in two steps. First, we define Δ as the optimization variable opposed to L. In this case the optimal configuration can be evaluated as the steady state of the following dynamical system, this generalizes the ideas proposed in [26]:

$$\begin{aligned}\dot{\Delta} &= J^{+}_{\text{set}} e_{\text{set}} \\ &+ (I - J^{+}_{\text{set}} J_{\text{set}}) J^{+}(x_{\text{ref}} - h(M^{-1}(\Delta + \Delta_0))),\end{aligned} \tag{5}$$

where $J^{+}(\Delta)$ is the Moore-Penrose pseudo-inverse of $J = \frac{\partial h(\Delta)}{\partial \Delta}$. $J_{\text{set}}, e_{\text{set}}$ are the Jacobian and the error of the constraints respectively. At any instant, J_{set} is obtained by selecting all the $i-$th columns of the identity matrix, such that the $i-$th row of $M^{-1}(\Delta + \Delta_0)$ is not in $[0, L_{\max}]$. e_{set} is equal to M^{T}_j if the variable violating the $j-$th violated constraint is below its lower bound, and is otherwise $-M^{\text{T}}_j$.

Once that the desired configuration is available, we can map it back to L coordinates using $L = M^{-1}(\Delta + \Delta_0)$. As such, the actuators configuration needs to satisfy:

$$L(x_{\text{d}}) = M^{-1}\left(\Delta_0 + \lim_{t \to \infty} \Delta(t; x_{\text{d}})\right) . \tag{6}$$

The limit is numerically evaluated through simulations as the steady state of (5). To map the length of each segment to the actual control signal to be sent to each of the servo-motors, $L(x_{\text{d}})$ needs to be pre-multiplied by the inverse of the block upper triangular matrix made from only of three by three identity matrices. Currently, the control commands are sent in an open loop configuration. However, posture sensing could be added, by introducing nonlinear integration action into (5) by substituting the actual posture of the robot to all the Δ appearing in the right side of the differential equations. We will explore closed loop control in future work.

III. FABRICATION & EXPERIMENTAL SETUP

The 3D printed tracks have been printed using a Fortus 250 Stratasys Printer. To create long sections simple interlocking

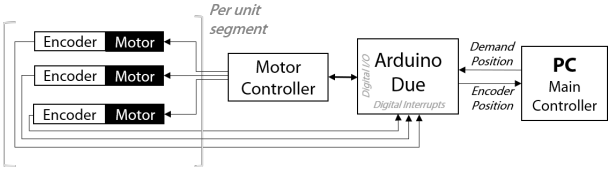

Fig. 6. System architecture of the control, showing the connections between the key components and also the flow of data through the system.

joints which were then permanently attached using a quick-dry Epoxy adhesive were created. The structure of the motorised segments was created by 3D printing housing and using Micro Metal DC motors and using a 398:1 gearbox used to power the mechanism. This gear ratio has been chosen to provide sufficient torque with a reasonable range of speed. Each motor is equipped with a quadrature encoder to enable both the direction and position to be determined with high precision. The gears were 3D printed to allow the tooth pitch and diameter to be customized to match that of the flexible racks.

The motors are controlled by H-bridges to provide speed and direction control. An Arduino Due microcontroller is used to control the H-bridges. The encoders are connected to digital interrupts on the microcontroller to allow continuous monitoring. A serial protocol has been developed to allow communication between the control program running on the PC and the Arduino. This allows a demand position to be set for each motor. The Arduino, then sets the direction and speed of the motor accordingly in order to move to the required encoder position. Appropriate motor speeds were choosen to overcome the frictional forces of the system whilst minimizing overshoot of the demand position. A block diagram of the system architecture is shown in Fig. 6.

IV. EXPERIMENTAL RESULTS

In this section we first characterize the performance of a single segment of the controller. The performance of the controller is then shown for a single segment. Finally, we present a demonstration of the capabilities of a multi-segments system.

A. Single Segment Characterization

To measure the range of movement possible with a single segment of the manipulator, the manipulator was moved to different starting lengths along the neutral axis, where each motor moved to length, l_0. The length of two of the three tracks is then reduced in small intervals, with the opposing track length increased until the maximum bending is achieved. The position of the tip of manipulator in 2D space perpendicular to the plane of movement was recorded and plotted. The results from these different starting lengths are shown in Fig. 7, with each experiment repeated 3 times. The longer the starting length, the greater then range, and angles of motion that can be achieved. The results show reasonably symmetric behaviors in the positive and negative x direction, showing robustness of the system when bending

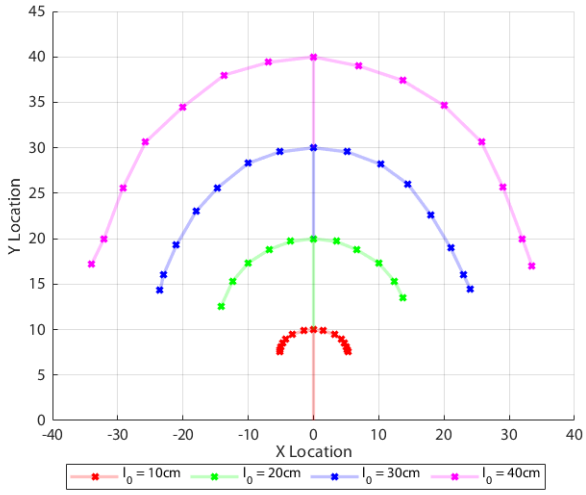

Fig. 7. Range of movement of a single segment when started from four different starting lengths.

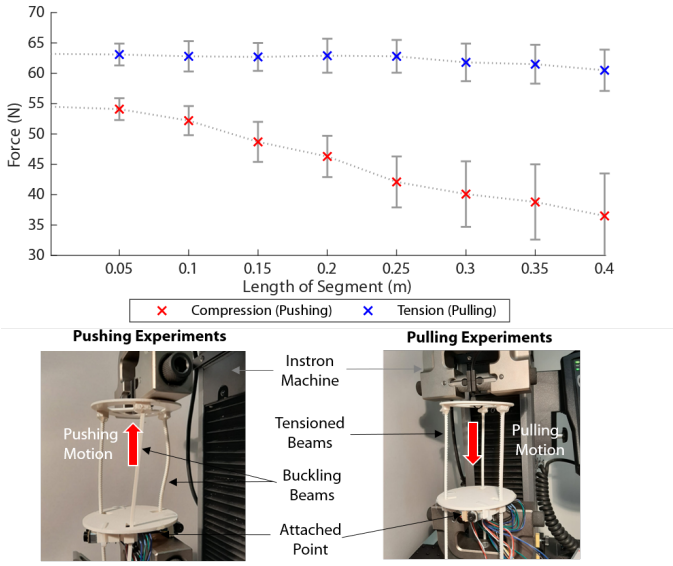

Fig. 8. Lifting and pulling forces of a single segment when tested using an Instron Machine. Each test was repeated 5 times with the average and standard deviation given.

using the different rack components in different bending modalities.

To identify the strength of a single segment in both a lifting and pushing modes, the force which can be applied by a single segment was measured using an Instron machine. The pushing and pulling forces which can be achieved with different starting lengths of the segment is shown in Fig. 8. Each experiment was repeated 5 times.

It can be seen that much higher forces can be achieved when the system in under load, as the 3D printed racks can support higher forces under tension in comparison to compression. Under compression the 3D printed tracks start to bend, this occurs earlier when the length of the segment is higher, resulting in the observed reduction of the compression force when the initial length of the segment is higher.

TABLE I

METRICS FOR MULTI-SEGMENTS AND SINGLE SEGMENT SYSTEM.

Metric	**Single Segment Actuation**	**Two Segment Actuation**
Maximum Speed of Extension	10 $\mathrm{cm\,s^{-1}}$	18 $\mathrm{cm\,s^{-1}}$
Reliability in Positioning	$\pm$19mm	$\pm$29mm
Range of Movement	65cm	80cm
Minimum Length	5cm	5cm
Maximum Length	65cm	82cm
Weight	-	0.6kg
Max Pulling Force	45N	75N

B. Single Segment Control

To demonstrate the capabilities of the controller, a single section manipulator ($\phi = \pi$) was moved along different motions paths. These motion paths for the center of the manipulator tip include: a) linear traverse, b) diagonal traverse and c) movement to four corners. Fig. 9 shows images of the positions reached along these motion paths for the three different motion paths. It can be seen that using only the encoder positions, the tip of the manipulator can be moved to a variety of different positions with reasonable precision with the operating area. Visually, it can be seen that the tip tracks along the desired trajectory.

C. Multi-Segment Demonstration

By introducing multiple moving segments, the reachability and the range of poses can be expanded. A manipulator with two segments has been created with tracks measuring approximately 1 meter in length. Fig. 10 shows a number of different poses which can be achieved with this multi-segment and also how the two segments can be moved independently to achieve different postures.

Table I records metrics for the multi-segment system for both a single segment and two segment actuation. These results reflect multiple experiments lasting over a period of quite some time.

In particular, the repeatability in positioning was investigated by measuring the position in 3D space that was reached when moving to a specific point from the retracted position five times. This was repeated for 3 different points in space, with an average error of $\pm$3cm in each dimension, showing reasonable repeatability. It can be seen that certain properties of segments are additive, for example maximum pulling force and speed, where as others do not scale with the the number of segments.

V. DISCUSSION & CONCLUSIONS

In this paper we presented a method for creating a manipulator structure which uses 3D printed flexible tracks to create a segment based manipulator. By tailoring the mechanical properties, namely the anisotropic stiffness, of the 3D printed tracks we can achieve both high force and also a large range of movement. A fundamental limitation

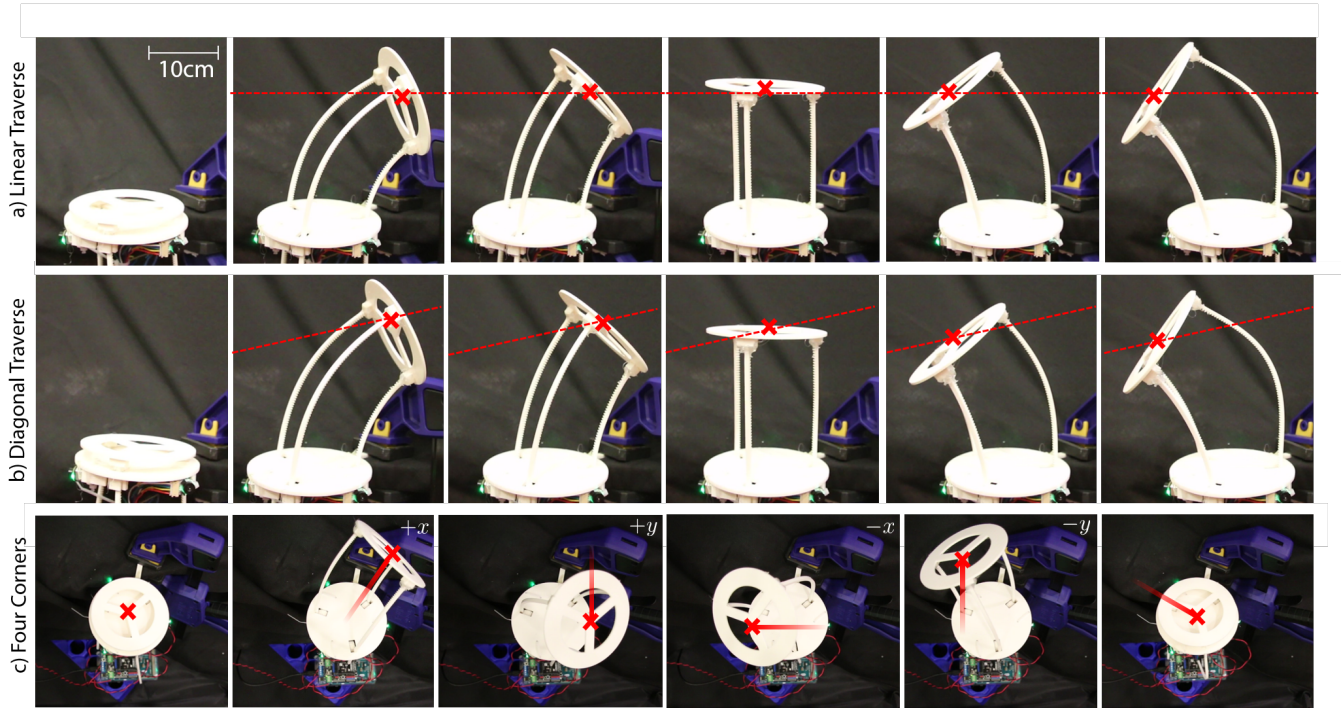

Fig. 9. Position of a single section manipulator as the controller is used to move the end point in three different motion paths. A) Straight traverse, B) Diagonal traverse and C) Movement to the four corner points.

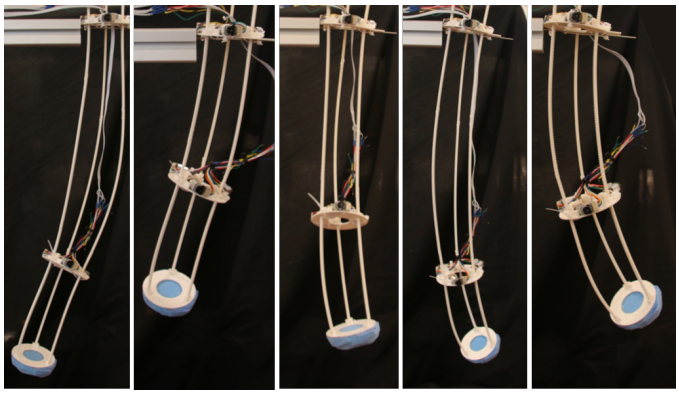

Fig. 10. Example postures that can be achieved using the multi-segment system.

of this approach is the need to include rigid parts along the manipulator. However, unlike softer systems, many of which are pneumatically or tendon operated, there is no need for additional outer compressors or air supplies and the system is entirely self-contained. This enables the system to show growth like behaviours.

Using an open-loop controller the ability to control the end tip position was shown. This was possible using only the encoders on the DC motors. By including more sensing modalities, such as using Inertial measurement units (IMUs) on the segments, this would allow closed-loop control to be implemented, improving the controllability and achievable precision of the system. This would also allow contact to be distinguished to assist with identifying information as to the environment.

This work demonstrates using an inherently rigid 3D printed structure to fabricate more compliant structures. This allows for more traditional and well understood techniques, such as single material 3D printing to be used to create softer more compliant robots. Such 'hybrid' robotic systems leverage both rigid and more compliant components to create structures which can apply both high forces, but also show deformability. It is a practical approach as allows more typical materials and fabrication approaches to be used, and enables capabilities which entirely soft systems could not achieve. Going forwards, a key research question is to the extent of the composition of this hybrid mix [22], [27]. Platforms such as this allow this trade-off to be investigated.

The fabrication and control approaches developed in this work can be extended to develop manipulators which can apply significant force, show length change and a wide range of movement. By integrating more moving platforms, developing increasingly robust and compliant 3D tracks and integrating more sensors to enable closed loop control this manipulator, the concepts can be developed into a multi-segment robotic manipulators. In comparison to existing state of the art systems, this approach can offer significant extensibility whilst also offering high controllability and the ability to apply significant forces. These capabilities could enable the system to perform manipulation tasks such as extending into hard to navigate spaces such as drawers, cupboards or shelving to remove heavy objects, or navigating through foliage to remove fruit from trees. These are tasks which would be challenging to achieve with existing technologies.

ACKNOWLEDGMENT

We would like to acknowledge support from grant NSF-EFRI 1830901 which enabled this research.

REFERENCES

[1] W. M. Kier and K. K. Smith, "Tongues, tentacles and trunks: the biomechanics of movement in muscular-hydrostats," *Zoological journal of the Linnean Society*, vol. 83, no. 4, pp. 307–324, 1985.

[2] B. Mazzolai, L. Margheri, M. Cianchetti, P. Dario, and C. Laschi, "Soft-robotic arm inspired by the octopus: Ii. from artificial requirements to innovative technological solutions," *Bioinspiration & biomimetics*, vol. 7, no. 2, p. 025005, 2012.

[3] T. Ranzani, G. Gerboni, M. Cianchetti, and A. Menciassi, "A bioinspired soft manipulator for minimally invasive surgery," *Bioinspiration & biomimetics*, vol. 10, no. 3, p. 035008, 2015.

[4] I. D. Walker, H. Choset, and G. S. Chirikjian, "Snake-like and continuum robots," in *Springer Handbook of Robotics*. Springer, 2016, pp. 481–498.

[5] D. Rus and M. T. Tolley, "Design, fabrication and control of soft robots," *Nature*, vol. 521, no. 7553, pp. 467–475, 2015.

[6] A. D. Marchese, R. K. Katzschmann, and D. Rus, "A recipe for soft fluidic elastomer robots," *Soft Robotics*, vol. 2, no. 1, pp. 7–25, 2015.

[7] M. E. Giannaccini, C. Xiang, A. Atyabi, T. Theodoridis, S. Nefti-Meziani, and S. Davis, "Novel design of a soft lightweight pneumatic continuum robot arm with decoupled variable stiffness and positioning," *Soft robotics*, vol. 5, no. 1, pp. 54–70, 2018.

[8] J. L. C. Santiago, I. S. Godage, P. Gonthina, and I. D. Walker, "Soft robots and kangaroo tails: modulating compliance in continuum structures through mechanical layer jamming," *Soft Robotics*, vol. 3, no. 2, pp. 54–63, 2016.

[9] J. D. Greer, T. K. Morimoto, A. M. Okamura, and E. W. Hawkes, "Series pneumatic artificial muscles (spams) and application to a soft continuum robot," in *2017 IEEE International Conference on Robotics and Automation (ICRA)*. IEEE, 2017, pp. 5503–5510.

[10] A. Shiva, A. Stilli, Y. Noh, A. Faragasso, I. De Falco, G. Gerboni, M. Cianchetti, A. Menciassi, K. Althoefer, and H. A. Wurdemann, "Tendon-based stiffening for a pneumatically actuated soft manipulator," *IEEE Robotics and Automation Letters*, vol. 1, no. 2, pp. 632–637, 2016.

[11] F. Maghooa, A. Stilli, Y. Noh, K. Althoefer, and H. A. Wurdemann, "Tendon and pressure actuation for a bio-inspired manipulator based on an antagonistic principle," in *2015 IEEE International Conference on Robotics and Automation (ICRA)*. IEEE, 2015, pp. 2556–2561.

[12] A. K. Mishra, E. Del Dottore, A. Sadeghi, A. Mondini, and B. Mazzolai, "Simba: Tendon-driven modular continuum arm with soft reconfigurable gripper," *Frontiers in Robotics and AI*, vol. 4, p. 4, 2017.

[13] E. W. Hawkes, L. H. Blumenschein, J. D. Greer, and A. M. Okamura, "A soft robot that navigates its environment through growth," *Science Robotics*, vol. 2, no. 8, p. eaan3028, 2017.

[14] A. Sadeghi, A. Mondini, and B. Mazzolai, "Toward self-growing soft robots inspired by plant roots and based on additive manufacturing technologies," *Soft robotics*, vol. 4, no. 3, pp. 211–223, 2017.

[15] A. Sadeghi, E. Del Dottore, A. Mondini, and B. Mazzolai, "Passive morphological adaptation for obstacle avoidance in a self-growing robot produced by additive manufacturing," *Soft robotics*, 2019.

[16] J. D. Greer, T. K. Morimoto, A. M. Okamura, and E. W. Hawkes, "A soft, steerable continuum robot that grows via tip extension," *Soft robotics*, vol. 6, no. 1, pp. 95–108, 2019.

[17] C. Della Santina, R. K. Katzschmann, A. Bicchi, and D. Rus, "Model-based dynamic feedback control of a planar soft robot: trajectory tracking and interaction with the environment," *The International Journal of Robotics Research*, p. 0278364919897292, 2019.

[18] L. Scimeca, J. Hughes, P. Maiolino, and F. Iida, "Model-free soft-structure reconstruction for proprioception using tactile arrays," *IEEE Robotics and Automation Letters*, vol. 4, no. 3, pp. 2479–2484, 2019.

[19] R. K. Katzschmann, C. Della Santina, Y. Toshimitsu, A. Bicchi, and D. Rus, "Dynamic motion control of multi-segment soft robots using piecewise constant curvature matched with an augmented rigid body model," in *2019 2nd IEEE International Conference on Soft Robotics (RoboSoft)*. IEEE, 2019, pp. 454–461.

[20] D. Trivedi, A. Lotfi, and C. D. Rahn, "Geometrically exact models for soft robotic manipulators," *IEEE Transactions on Robotics*, vol. 24, no. 4, pp. 773–780, 2008.

[21] A. Kanada, F. Giardina, T. Howison, T. Mashimo, and F. Iida, "Reachability improvement of a climbing robot based on large deformations induced by tri-tube soft actuators," *Soft robotics*, 2019.

[22] J. Hughes and F. Iida, "3d printed sensorized soft robotic manipulator design," in *Annual Conference Towards Autonomous Robotic Systems*. Springer, 2017, pp. 627–636.

[23] J. Z. Gul, M. Sajid, M. M. Rehman, G. U. Siddiqui, I. Shah, K.-H. Kim, J.-W. Lee, and K. H. Choi, "3d printing for soft robotics–a review," *Science and technology of advanced materials*, vol. 19, no. 1, pp. 243–262, 2018.

[24] R. J. Webster III and B. A. Jones, "Design and kinematic modeling of constant curvature continuum robots: A review," *The International Journal of Robotics Research*, vol. 29, no. 13, pp. 1661–1683, 2010.

[25] C. Della Santina, A. Bicchi, and D. Rus, "On an improved state parametrization for soft robots with piecewise constant curvature and its use in model based control," *IEEE Robotics and Automation Letters*, 2020.

[26] ——, "Dynamic control of soft robots with internal constraints in the presence of obstacles," in *Intelligent Robots and Systems (IROS 2019), 2019 IEEE/RSJ International Conference on*, 2019.

[27] J. Hughes, P. Maiolino, and F. Iida, "An anthropomorphic soft skeleton hand exploiting conditional models for piano playing," *Science Robotics*, vol. 3, no. 25, p. eaau3098, 2018.